We are IntechOpen, the world's leading publisher of Open Access books Built by scientists, for scientists

6,900
Open access books available

185,000
International authors and editors

200M
Downloads

Our authors are among the

154
Countries delivered to

TOP 1%
most cited scientists

12.2%
Contributors from top 500 universities



WEB OF SCIENCE™

Selection of our books indexed in the Book Citation Index in Web of Science™ Core Collection (BKCI)

Interested in publishing with us?
Contact book.department@intechopen.com

Numbers displayed above are based on latest data collected.
For more information visit www.intechopen.com



Chapter 7

Infrared and Raman Spectroscopic Characterization of Porphyrin and its Derivatives

Metin Aydin and Daniel L. Akins

Additional information is available at the end of the chapter

http://dx.doi.org/10.5772/64582

Abstract

Density functional theory (DFT) was employed to investigate protonation, deuteration, and substitution effects on the vibrational spectra of porphyrin molecules. The results of the calculations were compared with experimental data. The calculations show that *meso*-substitutions produced a substantial shift in frequencies when the *meso*-carbons within the parent porphine are involved in the vibrational motion of molecules, while protonation of the N atoms leads to a significant blue shift when the H atoms covalent bonded to the N atoms that are substantially involved in the vibrational motion. Deuteration of N atoms at the porphyrin core is found to result not only in a red shift in the frequencies of the corresponding peaks below 1600 cm^{-1}, but also to generate new Raman bands of frequencies in the range of 2565–2595 cm^{-1}, resulting from N-D bond stretching. Also, the deuteration of O atoms within the sulfonato groups ($-SO_3^-$) results in a new peak at near 2642 cm^{-1} due to O-D bond stretching. Calculated IR spectra of the compounds studied here showed similar differences. Finally, we discuss solvent effects on the IR spectrum of TSPP.

Keywords: porphyrins, protonation, Raman, IR, DFT calculation

1. Introduction

Molecular vibrations may be induced through two well-known optical excitation processes. One is the absorption of photons and the other is the inelastic scattering of photons. Excitation of molecular vibration by absorption of photons is achieved by irradiation of a species using radiation containing photons of a frequency equivalent to the frequency difference $\Delta\nu$ between the initial (i) and the final (f) vibrational states of the species; i.e., $\Delta\nu = \nu_f - \nu_i$. Unlike IR spectroscopy, the scattering mechanism for exciting molecular vibrations generally exploits monochromatic radiation. In this latter case, a number of incident photons is scattered

INTECH
open science | open minds

© 2016 The Author(s). Licensee InTech. This chapter is distributed under the terms of the Creative Commons Attribution License (http://creativecommons.org/licenses/by/3.0), which permits unrestricted use, distribution, and reproduction in any medium, provided the original work is properly cited. CC BY

inelastically such that the frequency of the scattered photons (ν_S) differs from that of the incident photons (ν_0). And with conversation of the energy, this energy difference is the energy change associated with a transition from the initial (i) vibrational state to the final (f) vibrational state of the scattering species; i.e., $\nu_0 - \nu_S = \nu_f - \nu_i$. Inelastic scattering of the photons was first discovered by the Indian scientist C. V. Raman in 1928 and is referred to as the Raman effect.

In this chapter, we discuss IR and Raman spectra of protonated, deuterated, and *meso*-substituted parent porphyrin using density functional theory (DFT) to calculate the IR and Raman spectra, and, where possible, make comparison to experimental spectra. We also discuss spectra of aggregates involving several of the porphyrin species, using vibrational band assignments to ascertain which motions of the vibrating molecule couple more effectively, with excitonic motion, and as a result, we derive molecular alignment information from the enhancement that certain vibronic bands in the Raman spectrum experience for the various porphyrins.

2. Overview of Raman spectroscopy

In this section, we focus on Raman scattering. It is convenient to define the Raman scattering cross-section for the n → m vibrational transition as $\sigma_{n\to m}$, and to relate it to the scattering intensity as follows:

$$\mathbf{I_{n\to m} = \sigma_{n\to m} I_0} \tag{1}$$

In this equation, $\mathbf{I_0}$ is the intensity of the incident radiation and $\mathbf{I_{n\to m}}$ the intensity of the light scattered by molecules integrated over all scattering angles and polarization directions for randomly oriented molecules. The Raman cross-section is associated with the Raman polarizability by utilizing the fact that the intensity for electric dipole radiation scales as the fourth power of the frequency:

$$\boldsymbol{\sigma_{n\to m} \propto (\nu_0 \mp \nu_k)^4 \sum_{\rho,\sigma} |\alpha_{\rho\sigma}|^2} \tag{2}$$

In this equation, the indices ρ and σ indicate the molecule-fixed directional coordinates. Moreover, for this equation, the scattering tensor $\alpha_{\rho\sigma}$ can be formulated in terms of Kramers -Heisenberg-Dirac dispersion theory, as indicated in Eq. (3) below [1]:

$$\left[\boldsymbol{\alpha_{\rho\sigma}}\right]_{nm} = \frac{1}{h}\sum_{S,r}\left\{\frac{\langle nG|M_\rho|Sr\rangle\langle rS|M_\sigma|Gm\rangle}{\nu_{Sr}-\nu_k-\nu_0+i\Gamma_S} + \frac{\langle rS|M_\sigma|Gm\rangle\langle nG|M_\rho|Sr\rangle}{\nu_{Sr}-\nu_k+\nu_0+i\Gamma_S}\right\}, \tag{3}$$

where M_ρ and M_σ represent the electronic transition dipole moment in a molecule-fixed coordinate system (Albrecht [2] and Warshel and Dauber [3]). The symbols ν_0 and ν_k represent the frequencies of the excitation radiation and the normal mode Q_k, respectively, S and r

http://dx.doi.org/10.5772/64582

represent the respective electronic and vibrational states of the molecule, and Γ_s is a damping constant, which is associated with the lifetime of the vibroelectronic state Sr. The sum in Eq. (3) indicates that for the Raman transition of all vibronic states must be used, which indicates that the scattering tensor, and thus, the Raman intensity, is controlled by the transition probabilities involving all vibronic states, even though the initial and final states refer to the vibrational ground and excited states of the electronic ground state. Thus, the sum of integrals in Eq. (3) describes the transitions: $|nG\rangle \rightarrow |Sr\rangle$ and $|Sr\rangle \rightarrow |Gn\rangle$. When the excitation frequency ν_0 is in resonance or preresonance with the frequency of an electronic transition, the scattering is referred to as resonance Raman (RR) scattering. In this case, Eq. (3) may be simplified to:

$$\left[\alpha_{\rho\sigma}\right]_{nm} \cong \frac{1}{h}\sum_{S,r}\left\{\frac{\langle nG|M_\rho|Sr\rangle\langle rS|M_\sigma|Gm\rangle}{\nu_{Sr}-\nu_k-\nu_0+i\Gamma_S}\right\}, \tag{4}$$

where the summation is now restricted to the vibrational states r of the resonantly excited electronic state (Albrecht [2]; Warshel and Dauber [3]). The wave functions of the integrals in Eq. (4) depend on the electronic and nuclear coordinates and may be separated by taking into account the Born-Oppenheimer approximation:

$$\langle nG|M_\rho|Sr\rangle = \langle G|M_\rho|S\rangle\langle n|r\rangle = M_{GS,\rho}\langle n|r\rangle \tag{5}$$

Here, the $\langle n|r\rangle$ integral represents the Franck-Condon factor, which is the integral over the product of two vibrational wave functions. With this approximation, Eq. (4) becomes:

$$\left[\alpha_{\rho\sigma}\right]_{nm} \cong \frac{1}{h}\sum_{r}\left\{\frac{M_{GS,\rho}M_{GS,\sigma}\langle n|r\rangle\langle r|m\rangle}{\nu_{Sr}-\nu_k-\nu_0+i\Gamma_S}\right\}, \tag{6}$$

where $M_{GS,\rho}$ is the electronic transition-dipole moment associated with the electronic transition from the ground state G to the electronically excited state S. Thus, $M_{GS,\rho}$ can be expanded in a Taylor series with respect to the normal coordinates Q_k:

$$M_{GS,\rho}(Q_k) = M_{GS,\rho}\left(Q_k^0\right) + \sum_k Q_k\left(\frac{\partial M_{GS,\rho}}{\partial Q_k}\right)_0 + \cdots \tag{7}$$

And, within the harmonic approximation, we neglect higher order terms and combine Eqs. (6) and (7) to obtain the scattering tensor as the sum of two terms, the so-called Albrecht A and B terms:

$$\left[\alpha_{\rho\sigma}\right]_{nm} \cong A_{\rho\sigma} + B_{\rho\sigma} + \ldots \tag{8}$$

$$A_{\rho\sigma} \cong \frac{1}{h}\sum_{r}\left\{\frac{M^0_{GS,\rho}M^0_{GS,\sigma}\langle n|r\rangle\langle r|m\rangle}{\nu_{Sr}-\nu_k-\nu_0+i\Gamma_S}\right\} \tag{9}$$

$$\mathbf{B_{\rho\sigma}} \cong \frac{\mathbf{1}}{\mathbf{h}}\sum_{\mathbf{r}}\left\{\frac{\mathbf{M^0_{GS,\sigma}}\left(\frac{\partial \mathbf{M_{GS,\rho}}}{\partial \mathbf{Q_k}}\right)_0\langle \mathbf{n}|\mathbf{Q_k}|\mathbf{r}\rangle\langle \mathbf{r}|\mathbf{m}\rangle}{\nu_{\mathbf{Sr}}-\nu_{\mathbf{k}}-\nu_{\mathbf{0}}+\mathbf{i}\Gamma_{\mathbf{S}}} + \frac{\mathbf{M^0_{GS,\rho}}\left(\frac{\partial \mathbf{M_{GS,\sigma}}}{\partial \mathbf{Q_k}}\right)_0\langle \mathbf{r}|\mathbf{Q_k}|\mathbf{m}\rangle\langle \mathbf{n}|\mathbf{r}\rangle}{\nu_{\mathbf{Sr}}-\nu_{\mathbf{k}}-\nu_{\mathbf{0}}+\mathbf{i}\Gamma_{\mathbf{S}}}\right\} \tag{10}$$

In the above equations, $M^0_{GS,\rho}$ and $M^0_{GS,\sigma}$ are the components of transition dipole moment of the vertical electronic transition G → S.

The A and B terms represent different scattering mechanisms, but the dominators are minimized in both terms when the frequency of the excitation v_0 is in preresonance or resonance with the frequency of an electronic transition. In such a case, both the A and the B terms are enhanced, leading to amplified scattering of radiation.

It is to be noted that if the resonant electronic transition exhibits a large oscillator strength, i.e., a large transition dipole moment $\mathbf{M^0_{GS}}$, then the A term may be increased substantially more than the B term, and therefore become the more important scattering term. In this case, the enhancement of a normal mode depends on the products of Franck-Condon factors, i.e., the term $\langle \mathbf{n}|\mathbf{r}\rangle\langle \mathbf{r}|\mathbf{m}\rangle$. It is to be noted that whether or not a normal mode is resonance enhanced via the Franck-Condon mechanism depends on the geometry of the resonant excited state.

The intensity of a vibrational band attributable to a normal mode Q of frequency v_Q can be estimated in the double harmonic approximation. For the nonresonant situation (for a normal mode $\mathbf{Q_K}$ of frequency v_{Qk} and excitation frequency v_0), the Raman intensity $\mathbf{I_{Qk}}$ can be computed according to the following equations [1, 4]:

$$\mathbf{I_{Q_k}} = \frac{\mathbf{f}\left(\nu_0-\nu_Q\right)^4}{\nu_{\mathbf{Q_k}}\left[\mathbf{1}-\mathbf{exp}\left(-\frac{\mathbf{h}\nu_\mathbf{Q}}{\mathbf{kT}}\right)\right]}\mathbf{S_{Q_k}} \tag{11}$$

$$\mathbf{S_{Q_k}} \cong \left\{\mathbf{45}\left(\frac{\partial \boldsymbol{\alpha}}{\partial \mathbf{Q_k}}\right)^2 + \mathbf{7}\left(\frac{\partial \boldsymbol{\gamma}}{\partial \mathbf{Q_k}}\right)^2\right\} \tag{12}$$

$$\left(\frac{\partial \boldsymbol{\alpha}}{\partial \mathbf{Q_k}}\right)^2 = \left(\frac{\mathbf{1}}{\mathbf{3}}\right)\left\{\left(\frac{\partial \boldsymbol{\alpha_X}}{\partial \mathbf{Q_k}}\right) + \left(\frac{\partial \boldsymbol{\alpha_Y}}{\partial \mathbf{Q_k}}\right) + \left(\frac{\partial \boldsymbol{\alpha_Z}}{\partial \mathbf{Q_k}}\right)\right\}^2 \tag{13}$$

$$\left(\frac{\partial \boldsymbol{\gamma}}{\partial \mathbf{Q_k}}\right)^2 = \left(\frac{\mathbf{1}}{\mathbf{2}}\right)\left\{\left[\left(\frac{\partial \boldsymbol{\alpha_X}}{\partial \mathbf{Q_k}}\right) - \left(\frac{\partial \boldsymbol{\alpha_Y}}{\partial \mathbf{Q_k}}\right)\right]^2 + \left[\left(\frac{\partial \boldsymbol{\alpha_Y}}{\partial \mathbf{Q_k}}\right) - \left(\frac{\partial \boldsymbol{\alpha_Z}}{\partial \mathbf{Q_k}}\right)\right]^2 + \left[\left(\frac{\partial \boldsymbol{\alpha_Z}}{\partial \mathbf{Q_k}}\right) - \left(\frac{\partial \boldsymbol{\alpha_X}}{\partial \mathbf{Q_k}}\right)\right]^2\right\} \tag{14}$$

In the above equations, $\mathbf{S_{Q_k}}$ is the Raman activity for a normal mode $\mathbf{Q_k}$, $\left(\frac{\partial \boldsymbol{\alpha}}{\partial \mathbf{Q}}\right)$ and $\left(\frac{\partial \boldsymbol{\gamma}}{\partial \mathbf{Q}}\right)$ are, respectively, the derivatives of the polarizability tensor and the corresponding anisotropy with respect to the normal mode Q, and f is a physical constant that includes the intensity of the incident radiation. We have calculated Raman intensities of the Raman active modes using Eq. (11), which is implemented in Gauss Sum software [5]. The software provides $\mathbf{S_{Q_k}}$ (the Raman activity, Eq. 12) and the frequency v_{Qk} from the output files of the quantum chemical calculation program (specifically, Gaussian 09).

http://dx.doi.org/10.5772/64582

We explore in this chapter the effect of protonation, deuteration, and *meso*-substitutions on the vibronic spectra of porphyrin and some of its derivatives. Specific molecules considered are the following: parent porphyrin (FBP), diprotonated FBP (H_4FBP), deuterated H_4FBP (D_4FBP); *meso*-tetraphenylporphyrin (TPP), diprotonated TPP (H_4TPP or dicationic TPP) deuterated H_4TPP (D_4TPP); *meso*-tetrakis (*p*-sulfonatophenyl) porphyrin (TSPP), diprotonated TSPP (H_4TSPP or dianionic TSPP), deuterated H_4TSPP (D_4TSPP), dicationic TSPP (H_8TSPP), as well as deuterated H_8TSPP (D_8TSPP). We also deal with how molecular aggregation of some of the aforementioned species affects Raman spectra. Density functional theory has been employed to calculate the vibronic structural properties for both IR and Raman spectra.

Our motivation for focusing on the porphyrin monomers and aggregates is that porphyrin monomers and their aggregates play fundamental roles in natural systems and increasingly in artificial photonic devices. As regards aggregates, the primary mechanism through which molecular aggregate structures are formed in both natural and artificial systems is self-assembly through intrinsic intermolecular interactions, without the formation of covalent linkages. Self-assembled molecular aggregates often assume a structure that can be classified as being of J- or H-type, defined by the relative orientations of induced transition dipoles of the constituent molecules, either "head-to-tail" or "head-to-head," respectively [6]. Structural pictures such as those provided by J- and H-aggregates have provided a framework for theoretical analysis of structure and dynamics of aggregated systems.

Moreover, aggregated porphyrin species are model composite structures for gaining insight into the roles that optically induced transient structural changes and photon dynamics play in photosynthesis [7, 8]. And through the study of spectral properties and photodynamic behaviors of aggregated porphyrin structures, an important outcome sought is the translation of the electron transfer specificities and speeds often found for biological reactions to the realm of molecular photonic devices (i.e., biomimetics) or photonic materials; indeed, enormous interest in the applications area has been evidenced [9, 10]. Thus, experimental and quantum chemical calculations of structures and optical dynamics of porphyrin monomers and aggregates have both scientific and technological importance.

We deduce that the observed Raman bands of the TPP, TSPP, H_4TSPP, and aggregated H_4TSPP may most properly be characterized by the vibrations of the pyrrole and pyrroline rings, the sulfonatophenyl groups, and their combinations rather than as vibrations of isolated chemical bonds.

As regards IR spectra, we have found that calculated IR spectra of H_4TSPP can be assigned by comparison with the calculated IR spectra of other porphyrin derivatives and the experimentally measured IR spectra that are obtained from the literature. We further point out that the experimental and theoretical data used in this chapter are taken from prior experimental measurements performed in our laboratories [11–13].

The Raman and IR spectra of porphyrin derivatives in water, used as solvent in the calculations, were calculated at the B3LYP/6-311G (d, p) level of density functional theory.

3. The Raman spectra of porphyrin and derivatives

Figure 1 provides the measured Raman spectra of the TPP (**Figure 1B**) and H_4TSPP (**Figure 1G**) from our previous works [11–13]. Many Raman bands with strong and medium intensity, as well as numerous weak bands are found throughout the spectrum. The Raman spectrum of the H_4TSPP when compared to that of the TPP are quite similar, however, the positions of several bands are substantially shifted in frequency. As examples, in the observed Raman spectrum of the TPP, the strongest band at 1564 cm^{-1} and the bands at 334, 1234, 1327, 1438, 1577, and 1595 cm^{-1} (with relatively weak intensity) are respectively red shifted to 1537 cm^{-1} (the most intense peak), 312, 1229, 1339, 1427, 1562, and 1494 cm^{-1} in the H_4TSPP spectrum. Also, the bands at 201, 334, 962, and 1002 cm^{-1} are respectively blue shifted to 236, 314, 983, and 1014 cm^{-1} in the H_4TSPP spectrum. Additionally, the bands at 1476 and 701 cm^{-1} in the H_4TSPP spectrum are considerably enhanced compared to their corresponding ones in the TPP.

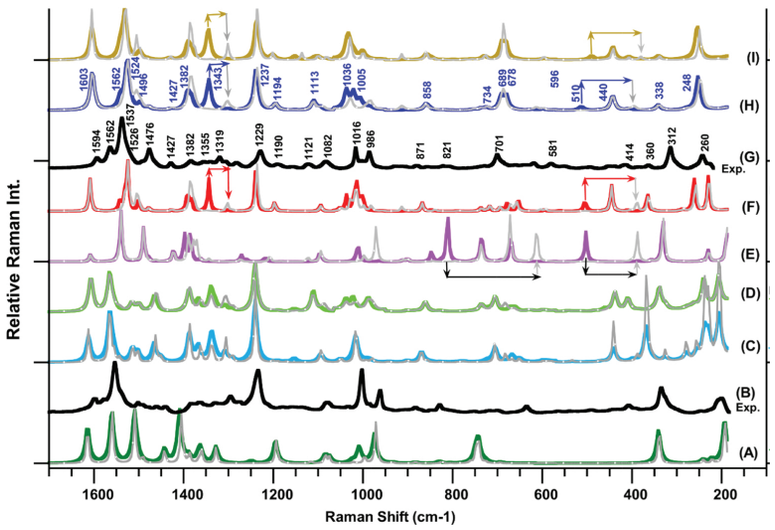


Figure 1. The predicted Raman spectra of porphyrin derivatives: (**A**) free-base porphyrin (FBP) and deuterated FBP (D_2FBP); (B) the experimentally measured Raman spectrum of the TPP; (**C**) *meso*-tetraphenylporphyrin (TPP) and (D_2TPP); (**D**) anionic *meso*-tetrakis(*p*-sulfonatophenyl)porphyrin (TSPP) and deuterated TSPP (D_2TSPP); (**E**) diprotonated FBP (H_4FBP) and deuterated H_4FBP (D_4FBP); (**F**) diprotonated-TPP (H_4TPP) and deuterated H_4TPP (D_4TPP); (**H**) diprotonated TSPP (H_4TSPP) and deuterated-H_4TSPP (D_4TSPP); and (**I**) dicationic TSPP (H_8TSPP) and deuterated H_8TSPP (D_8TSPP). The plotted spectra in the gray color belong to the deuterated molecules. The calculations were carried out in water at B3LYP/6-311G(d, p) level of DFT, and the line arrows show the frequency shift in the deuterated molecule [11].

Also, calculated Raman spectra of the FBP/D_2FBP, H_4FBP/D_4FBP, TPP/D_2TPP, H_4TPP/D_4TPP, TSPP/D_2TSPP, H_4TSPP/D_4TSPP, and H_8TSPP/D_8TSPP in water used as a solvent are given in **Figure 1**, with the observed Raman spectra of the TPP and H_4TSPP for comparison. (It is important to note that the D_8TSPP symbolize the dicationic TSPP where four of eight deuterium atoms (D) covalently bounded to the nitrogen atoms at the core and the other four covalent bonded to one of three oxygen atoms within each of four *meso*-sulfonatophenyl substituted groups.)

TPP						TSPP				H_4TSPP						Assignments
Sym	$\Delta\nu_{sc.}$	S_R	I_R	$\Delta\nu_{exp}$	$I_{R/exp}$	Sym	$\Delta\nu_{sc.}$	S_R	I_R	Sym	$\Delta\nu_{sc.}$	S_R	I_R	$\Delta\nu_{exp}$	$I_{R/exp}$	
A2	1612	25	24	1595	29	A2	1607	44	42	A2	1603	45	40	1593	21	C-C bond stretching within phenyl rings and rocking of their H, no any contribution comes from mac-
A1	1612	29	27			A1	1607	53	50	A1	1603	55	49			rocycle and sulfonato groups (-SO_3^-) (-SO^-_3).
A1	1588	<1	<1	1577	27	A1	1574	1	1	A1	1568	2	1	1563	42	C-C bond stretching within phenyl rings and rocking of their H, accompanied by relatively weak asymmetric stretching of C_α-C_m-C_β bond stretching, no any contribution comes from sulfonato groups.
A1	1564	100	100	1553	100	A1	1564	100	100	A1	1524	100	100	1537	100	C_β-C_β bond stretching, $\nu(C_\beta$-$C_\beta)$, symmetric stretching of C_α-C_m-C_α bonds, $\nu_s(C_\alpha$-C_m-$C_\alpha)$ that leads to
				1540	40									1528	42	bending deformation of the C-N-C bonds, θ(C-N(H)-C).
A2	1559	8	8			A2	1558	9	9	A2	1540	29	28			$\nu_s(C_\alpha$-C_m-$C_\alpha)$/rocking of C-N(H)-C and H on N atoms, ρ(C-N(H)-C)/ρ(NH)
A1	1555	15	15			A1	1554	8	8	A1	1529	26	25			Asymmetric stretching of (C_α-C_m-C_α) bonds $\nu_a(C_\alpha$-C_m-$C_\alpha)$/θ(C-N(H)-C).
A1	1514	24	25	1502	21	A1	1515	21	23	A1	1477	5	5	1476	38	$\nu(C_\beta$-$C_\beta)$ and rocking of the H on C atoms within macrocycle (not on the phenyl groups), $\rho(C_\beta H)$, and relatively weak θ(C-N(H)-C)
A2	1502	14	15	1491	16	A2	1499	14	15	A1	1496	7	7	1489	15	ρ(CH within phenyl groups only)
A1	1501	4	4			A1	1498	3	4	A2	1495	8	8			
A2	1466	31	36	1461	13	A2	1464	37	44							$\nu(C_m$-$C_\alpha)/\rho(C_\beta H)$, and relatively weak ν_a(C-N(H)-C)
A1	1454	3	3	1438	12	A1	1454	2	2	A1	1426	3	3	1428	11	$\nu_s(C_\alpha$-C_m-$C_\alpha)$/ ρ(C-N(H)-C)/ρ(CH)
A2	1387	46	61	1378	20	A2	1387	44	58	A2	1391	31	38	1384	15	$\nu_a(C_\beta$-C_α-N(H))/$\rho(C_\beta H$-$C_\beta H)$
A1	1367	22	30			A1	1367	22	29	A1	1382	20	25	1354	14	$\nu(C_\beta$-$C_\alpha)$/θ(C-C_m-C)/θ(C-N(H)-C), which leading to macrocycle getting a square shape)
A2	1339	19	26	1327	20	A2	1338	42	60	A2	1343	52	70	1340	14	$\nu(C_\varphi$-$C_m)/\rho(C_\beta H)/\rho$(NH), and relatively weak ν_a(C-N(H)-C)
A2	1335	26	38			A2	1329	13	19					1319	22	
A1	1306	13	19			A1	1305	7	10	A1	1321	1	1	1304	14	ν_a(C-C-C) within phenyl groups/θ(C-N(H)-C)/ρ(CH).
A1	1291	4	7			A1	1290	4	6	A1	1300	1	2	1283	12	
A1	1239	75	127	1234	84	A1	1239	77	131	A1	1237	60	97	1229	34	$\nu(C_\varphi$-$C_m)$ (primarily)/ν_s(C-N(H)-C)/ρ(CH)/$\nu(C_\beta$-$C_\beta)$ (relatively weak)
A2	1189	0.	0.			A2	1188	1	1	A2	1194	3	6	1190	8	ρ(CH) within phenyl groups.
A1	1189	1	2			A1	1189	1	1	A1	1194	5	9			
A2	1152	4	8	1137	10	A2	1153	3	5							ρ(NH)/$\rho(C_\beta H)$ and relatively weak structural deformation
						A2	1146	<1	<1	A2	1151	<1	<1	1122	9	ν_a(O-S-O) within sulfonato groups
A1	1097	1	2	1080	21	A1	1109	19	42	A1	1108	9	18	1082	14	ν(S-O)/θ(C-C(S)-C) within sulfonato groups.
A1	1091	5	11			A1	1092	3	6	A1	1093	2	4			$\rho(C_\beta H)$
A1	1048	2	6			A1	1036	1	3	A1	1033	<1	1			θ(C-C-C) within the phenyl groups
A2	1013	6	15			A2	1037	1	4	A2	1035	1	3			

http://dx.doi.org/10.5772/64582

TPP						TSPP				H_4TSPP						Assignments
Sym	$\Delta\nu_{sc.}$	S_R	I_R	$\Delta\nu_{exp}$	$I_{R/exp}$	Sym	$\Delta\nu_{sc.}$	S_R	I_R	Sym	$\Delta\nu_{sc.}$	S_R	I_R	$\Delta\nu_{exp}$	$I_{R/exp}$	
A1	1020	4	10	1002	85	A1	1020	2	5	A1	1036	3	7	1016	40	Expansion of the pyrrole/pyrroline groups along N(H)…N(H) direction due to $\nu(C_\alpha\text{-}C_\beta)$, leading to macrocycle getting rectangular shape instead of square shape.
A1	983	2	4	962	44	A1	986	2	5	A1	1005	2	5	1002	15	Expansion of the pyrrole/pyrroline groups along N(H)…N(H) direction in the same phase like macrocycle getting square shape or similar to breathing of the macrocycle
A2	990	1	2			A2	988	1	2	A2	992	0.	1			Out of plane wagging of the H on the phenyl rings, w(CH)
A1	899	1	3			A1	899	1	3	A1	904	<1	1	986	32	Bending deformation inside entire molecule.
A1	868	3	13			A1	859	4	14	A1	858	2	8	879	6	w(CH on the macrocycle and phenyl rings)
A1	815	<1	<1			A1	814	<1	<1	A1	820	<1	1	821	5	
A1	768	<1	<1			A1	749	<1	1	A1	751	1	2			Out of plane bending deformation of whole molecule including w(CH/NH)
A1	727	<1	<1			A1	734	3	15	A1	734	1	5	728	5	ν(S-O) and expansion of the phenyl rings along S…C_m direction including w(CH/NH)
										A2	689	5	31	701	27	Out of plane twisting of the macrocycle
A1	665	2	12	636	13	A1	669	1.33	9	A1	678	5	33			
A1	584	<1	2			A1	589	<1	1	A1	596	<1	3	580	10	w(NH and CH on the macrocycle and phenyl rings) and wagging of the macrocycle.
A1	531	0.	3			A1	574	0.	1	A1	566	0.	1	548	5	Wagging of entire molecule
										A1	510	0.	2	494	3	w(NH)
A2	468	<1	1			A2	457	1	13	A2	468	<1	1			In-plane wagging of macrocycle and translational motion of phenyl rings.
A2	437	2	33	408	15	A2	435	2	25	A2	440	2	25	439	5	Out of plane bending of the phenyl rings.
						A1	407	2	47	A1	404	<1	6	414	8	Breathing macrocycle and translational motion of phenyl rings in opposite phase.
A1	365	6	160	334	50	A1	336	3	111	A1	338	1	24	314	41	Breathing of whole molecule.
A2	322	<1	17											363	7	Out of plane wagging of macrocycle.
A1	235	2	127	201	29	A1	237	2	152	A1	248	2	144	242	26	Out of plane wagging of macrocycle.
A1	252	<1	28			A1	257	<1	18	A1	252	<1	12			Out of plane wagging of phenyl rings and relatively weak out of plane wagging macrocycle.

The calculations were obtained in water used as solvent at B3LYP/6-311G(d,p) level. Where $\Delta\nu_{sc}$ symbolizes the scaled vibrational frequencies, $\Delta\nu_{sc.} = 0.96\ (\Delta\nu_{calc}) + 40$, and SR and IR represents, respectively, the predicted Raman scattering activity and intensity; and $\Delta\nu_{exp}$ and $I_{R/exp}$ symbolize the measured Raman frequency and Intensity, respectively [11–13].

Table 1. Predicted and measured Raman active modes of frequencies (in cm^{-1}) of the H_4TSPP (C_{2v}) with the TPP (C_{2v}) and TSPP (C_{2v}).

http://dx.doi.org/10.5772/64582

FBP	**H_4FBP**	**TPP**		**H_4TPP**	**TSPP**	**H_4TSPP**		**H_8TSPP**
Calc.	Calc.	Calc.	Exp.	Calc.	Calc.	Calc.	Exp.	Calc.
1007	1013	1020	1002	1036	1020	1036	1016	1036
972	1010	983	962	1002	985	1005	983	1001
D_2FBP	**D_4FBP**	**D_2TPP**	**D_4TPP**	**D_2TSPP**	**D_4TSPP**	**D_8TSPP**	**D_2FBP**	**D_4FBP**
Calc.	Calc.			Calc.	Calc.	Calc.	Exp. [14]	Calc.
996	995	1017		1026	1012	1026	1004	1026
968	968	979		980	977	983	957	979

Table 2. The predicted Raman active bands of frequencies (for the protonated and deuterated porphyrin derivatives) exhibited significant frequency shift in the range of 1040–950 cm^{-1}.

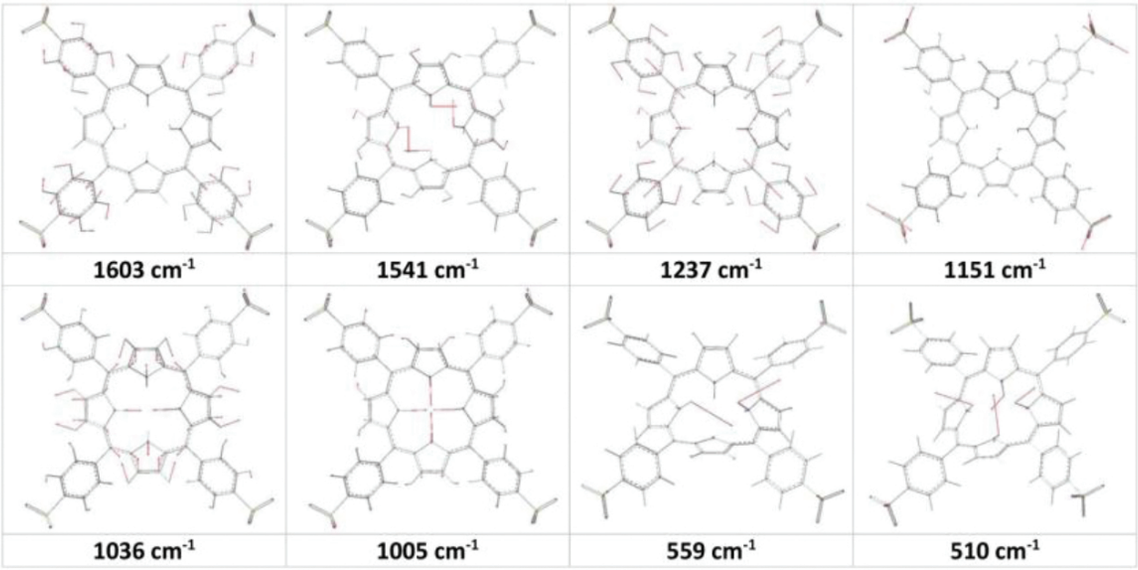


Figure 2. Calculated molecular motions for some vibrational bands of the H_4TSPP, from reference [11].

The assignment of the observed vibrational bands in the Raman spectra of the TPP and H_4TSPP were made based on the density functional prediction at the B3LYP/6-311G (d, p) level and on the atomic displacements visualized by using the GaussView program. The calculated vibrational frequencies coincided with those observed in their Raman spectra. We used the calculated frequencies and, to some degree, the predicted intensity distribution to attribute observed vibrational frequencies and intensities to specific intramolecular motions of the H_4TSPP and TPP. These latter assessments were facilitated by analysis of the calculated nuclear displacements, combined with animation of their vibrations, to identify specific motions as the dominant movements within the molecule. This is not a truly rigorous approach but should provide adequate insight. The assignments of the vibrational mode are provided in **Tables 1** and **3**, whereas **Figure 2** presents the nuclear displacement for several selected vibrational modes.

TPP						TSPP			H_4TSPP				H_8TSPP			Assignments
Sym	$\Delta\nu_{sc.}$[a]	$\Delta\nu_{sc.}$[b]	I_{IR}	$\Delta\nu_{exp}$ [15]	$\Delta\nu_{exp}$ [16]	Sym	$\Delta\nu_{sc.}$[a]	I_{IR}	Sym	$\Delta\nu_{sc.}$[a]	I_{IR}	$\Delta\nu_{exp}$ [16]	Sym	$\Delta\nu_{sc.}$[a]	I_{IR}	
B2	447	414	6	409	406	B2	431	1	B2	439	3	415	B2	439	1	In-plane rotational motion of the pyrroline rings, including relatively weak out-of-plane twisting deformation of the phenyl rings, but no contributions come from the pyrroline rings
						B2	438	13	B2	427	5	445				Rocking of phenyl rings (ρ(phenyl) and wagging of macrocycle w(macrocycle).
B2	447	414	6			B2	475	59	B2	439	3	457	B2	469	1	Out-of-plane bending of phenyl groups only.
B1	553	521	10		516	B1	523	2	A1	484	8		A1	484	8	Twisting of phenyl τ(phenyl) and w(macrocycle)
A1	584	553	2						A1	510	8		A1	487	4	w(NH only)
B2	570	539	2	559	558				B1	559	10		B1	567	10	
						A1	540	8	A1	566	14	560				Out of plane twisting of the molecule and θ(O-S-O)/w(CH and NH)
						B1	541	1	B1	567	6	580				
						B2	627	45	B2	624	63	637	B2	582	39	Due to bending deformation of the SO_3^- groups like closing and opening umbrella shape.
	647	618	2	619	618	A1	657	0.6								In plane bending deformation of phenyl rings, including w(NH and C_βH only) and out of plane deformation of the macrocycle.
A1	666	636	4	638	636	A1	668	1.0								
B2	688	659	6	658	657											
B2	728	700	43	699	701											w(CH on phenyl) and relatively weak out of plane deformation of the phenyl rings.
						B2	732	6	B2	722	12	715	B2	725	5	w(CH on phenyl) and out of plane deformation of the phenyl rings and macrocycle.
						B2	747	16	B2	748	19	741	B2	739	6	Primarily due to ν(S-C)/θ(phenyl) and relatively weak w(CH an NH) and out of plane bending (or twisting) deformation of macrocycle,
A1	745	716	61			A1	749	10	A1	751	6		A1	753	19	Primarily due to w(C_βHs an NH) and out of plane bending (or twisting) deformation of macrocycle, relatively weak out of plane deformation of the phenyl.
B2	757	729	32	727	728											w(C_βH an NH) and out of plane bending (or twisting) deformation of macrocycle, relatively weak out of plane deformation of the phenyl.
B1	776	749	37			B1	757									w(CH in phenyl and macrocycle) and out of plane bending (or twisting) deformation of phenyl rings the macrocycle.

TPP						TSPP			H_4TSPP				H_8TSPP			Assignments
Sym	$\Delta\nu_{sc.}$[a]	$\Delta\nu_{sc.}$[b]	I_{IR}	$\Delta\nu_{exp}$ [15]	$\Delta\nu_{exp}$ [16]	Sym	$\Delta\nu_{sc.}$[a]	I_{IR}	Sym	$\Delta\nu_{sc.}$[a]	I_{IR}	$\Delta\nu_{exp}$ [16]	Sym	$\Delta\nu_{sc.}$[a]	I_{IR}	
B2	776	749	21	746	748	B2	767	1								
													A1	769	32	Mainly due to ν(S-O(H)), including w(C_βHs an NH) and out of plane bending (or twisting) deformation of macrocycle, relatively weak out of plane deformation of the phenyl.
													B2	773	66	
A1	815	788	3	785	788	B1	823	7	B1	825	2	800	B1	826	3	W(C_βHs and NH) and out of plane bending deformation of macrocycle
A1	829	802	100	798	799	A1	829	20	A1	848	23	854	A1	852	15	
B1	894	869	10	875	871	B1	896	1								θ(N-C_α-C_β and N-$C_{\alpha'}$-$C_{\beta'}$ in the same phase)/θ(C_m-C_α-N)/θ(C_α-C_m-C_α)/θ(phenyl)/ρ(C_βH)
B1	985	960	91	964	962	B1	968	5	B1	974	1	966	B1	998	2	W(CH on phenyl)
						B2	980	63	B2	980	100	984				νs(O-S-O)
B2	1001	977	34			B2	1002	5	B2	1004	2	1012	B2	1004	9	θ(N-C_α-C_β and N-$C_{\alpha'}$-$C_{\beta'}$ in the same phase)/θ(C_m-C_α-N)/θ(C_α-C_m-C_α)/θ(phenyl)/ρ(C_βH)
A1	1020	996	0.	979	980	A1	1020	0.	A1	1036	2	1039	A1	1035	1	Expansion of the pyrrole/pyrroline groups along N(H)…N(H) direction due to ν(C_α-C_β), leading to macrocycle getting rectangular shape instead of square shape.
B1	1014	991	11													θ(C-C-C in phenyl)
B2	1016	993	33	999	1002	B2	1016	1								ρ(C_βH)/θ(C-C-C in phenyl)/θ(C_m-C_α-N)
B1	1049	1026	9	1031	1032				B1	1033	<1					ρ(CH in phenyl)/θ(C-C-C in phenyl)
B1	1087	1065	9	1069	1072				B1	1089	1					ρ(C_βH)
A1	1094	1072	10													ρ(C_βH and CH on phenyl).
						B1	1109	21	B1	1108	11		B1	1107	3	ν(C-S)/θ(C-C(S)-C)/ρ(CH on phenyl only)
						A1	1116	14	A1	1125	6	1125	A1	1133	1	ρ(CH on phenyl only)
						B2	1146	64	B1	1151	30					νa(O-S-O)
						A1/B1	1156	100	A1/B1	1160	35	1188a	A1/B1	1151	100	νa(O-S-O)/ρ(CH on phenyl)
B2	1180	1159	38		1155	B2	1180	8								νa(C-N-C)/θ(C-N-C)/ ρ(C_βH)
B2	1189	1168	4	1174	1176	B2	1188	0.	B2	1193	9		B2	1200	3	ρ(CH on phenyl only)
B1	1204	1183	25	1187	1187	B1	1204	4								ρ(NH) and relatively weak θ(whole molecule)
B2	1224	1203	13	1211	1211	B2	1224	2	B2	1220	14	1218	B2	1221	2	νs(C-N-C)/νs(C_φ-C_m-C_α)/ρ(NH and CH)

http://dx.doi.org/10.5772/64582

TPP						TSPP			H_4TSPP				H_8TSPP			Assignments
Sym	$\Delta\nu_{sc}$.[a]	$\Delta\nu_{sc}$.[b]	I_{IR}	$\Delta\nu_{exp}$ [15]	$\Delta\nu_{exp}$ [16]	Sym	$\Delta\nu_{sc}$.[a]	I_{IR}	Sym	$\Delta\nu_{sc}$.[a]	I_{IR}	$\Delta\nu_{exp}$ [16]	Sym	$\Delta\nu_{sc}$.[a]	I_{IR}	
B1	1235	1215	17	1220	1219	B1	1235	3	B1	1240	12		B1	1241	7	νa(C-N-C)/ρ(NH and C_βH)
B1	1262	1242	9	1247	1251	B1	1262	2	B1	1299	11		B1	1301	2	ν(C_β-C_α)/θ(C-N-C)/ρ(C_βH and NH).
B1	1355	1337	47	1348	1351	B1	1354	8	B1	1348	1	1350	B1	1387	1	νa(C_β-C_β-C_α)/ θ(C_α-N-C_α)/νa(C_φ-C_m-C_α)/θ(C_φ-C_m-C_α)/ρ(CH).
B1	1373	1356	24	1359	1358	B1	1373	4	B1	1386	5	1384	B1	1387	1	νa(C-N-C)/ρ(C_βH and NH).
B2	1411	1394	22	1400	1400	B2	1411	4								ν(C_β-C_α)/ν(C_α-C_m) which also leading to νa(C_β-C_α-C_m), including ρ(C_βH).
A1	1451	1435	12	1459	1437	B2	1399	2	B1	1405	9	1395	B1	1407	6	ρ(CH on phenyl), including relatively weak νs(C-C-C_φ)
B2	1482	1466	82	1471	1471	B2	1482	16	B2	1460	62	1472	B2	1467	17	N(C_β-C_β)/ν(C_α-C_m) that leading to θ(C-N-C)
B1	1492	1486	7	1488	1493											ν(C_α-C_m)/ν(C_β-$C_{\beta'}$)/νa(C_α-NH-C_β), including ρ(CH) on the macrocycle only.
B1	1568	1554	67		1555	B1	1567	10	B1	1545	1	1554	B1	1545	3	
B1	1588	1574	1	1573	1575				B2	1566	1	1558 1564				νa(C-C-C) within phenyl rings and ρ(H on phenyl)
B2	1612	1598	30	1595	1595	B2	1607	2	B1	1603	8	1592 1597	B2	1604	1	ν(C-C)/ρ(CH) within phenyl rings, including θ(C-C-C in phenyl).

Where $\Delta\nu_{sc}$ represents the scaled vibrational frequencies ((a) $\Delta\nu_{sc} = 0.96(\Delta\nu_{calc}) + 40$ as used for the Raman spectra for all compounds studied here) and I_{IR} symbolizes the predicted IR intensity. In the assignments, the symbols ν, θ, ρ, and w represent the bonding stretching, bending deformation, rocking, and wagging, respectively. It is worthy to note that two different scaling factor used for the TPP: (a) $\Delta\nu_{sc} = 0.96(\Delta\nu_{calc}) + 40$ and (b) $\Delta\nu_{sc} = 0.976(\Delta\nu_{calc})$. The latter one, (b), gives best fitting to measured IR spectrum (from ref. [15, 16]) of the TPP only; not for others. However, the scaling factor of $\Delta\nu_{sc} = 0.96(\Delta\nu_{calc}) + 40$ gives the best fitting to measured IR spectrum of H_4TSPP (from ref. [16]). The results of calculations were obtained in water used as solvent at the B3LYP/6-311G (d,p) level of the theory.

Table 3. Assigned IR features of the *meso*-substituted porphyrin derivatives: TPP (C_{2v} point group), TSPP (C_{2v}), H_4TSPP (C_{2v}), and H_8TSPP (C_{2v}).

http://dx.doi.org/10.5772/64582

Our assignments may be summarized as follows:

1. The observed Raman peak at 1593 cm^{-1}: The calculations, as shown in **Figure 1**, produce a peak at around 1600 cm^{-1} in the Raman spectra of all of the molecules studied here. The motions of atoms within the molecules suggest that this calculated band is as a result of principally C-C bond stretching, ν(C-C), within phenyl rings and rocking of their H, ρ(CH). No contribution appears to derive from the macrocycle and sulfonato groups ($-SO_3^-$) motions. Calculations for the parent porphyrin (FBP) and diprotonated FBP (H_4FBP) also predicted a band at about 1600 cm^{-1}, resulting from asymmetric stretching of the C_α-C_m-C_α (ν_a(C-C_m-C)) and bending deformation of the C-N(H)-C and C-N-C bonds, and rocking of H atoms covalent bonded to *meso*-carbon atoms (C_m), ρ(C_mH); see **Figure 2**. Consequently, we can conclude that the vibrational motion of the substituted phenyl is responsible for the observed Raman band at 1593 cm^{-1} in the observed spectrum of diprotonated TSPP (H_4TSPP). It is to be noted that, in our prior publication [13], the observed and predicted Raman spectra of the TPP showed the similar Raman pattern; these results are also presented in **Table 1** and **Figure 1**.

2. The experimental peak at 1563 cm^{-1}: Even though the measured Raman spectrum of the H_4TSPP displays a relatively weak bands at 1563 cm^{-1}, the calculation indicates only a very weak peak at 1568 cm^{-1}, attributed to C-C bond stretching within the phenyl rings and rocking of their attached H atoms, as well as a relatively weak asymmetric stretching of C_α-C_m-C_β bonds. However, there is no contribution from the sulfonato group. Upon examination of this peak for vibrational motions for the TPP, TSPP, H_4TPP, and H_8TSPP, we find extremely weak peaks at 1588, 1574, 1585, and 1578 cm^{-1}, respectively. As seen in **Figure 1** and **Table 1**, the calculated spectrum of the TSPP produces the most intense band at 1564 cm^{-1}, but its vibrational motions indicated that this mode is shifted to 1524 cm^{-1} in the H_4TSPP spectrum. Therefore, we believe that the DFT calculations might underestimate the intensity of this peak.

3. The observed strong Raman bands at 1553 cm^{-1} (with a shoulder at 1540 cm^{-1}) and at 1537 cm^{-1} (with a shoulder at 1528 cm^{-1}) are, respectively, in the spectra of TPP and H_4TSPP: Their calculated spectra display the strongest Raman band at 1564 and 1524 cm^{-1} for TPP and H_4TSPP, respectively. Both of experimental and calculated Raman spectra show that the strongest band in the observed spectrum of the TPP is significantly red shifted in the H_4TSPP. The large red shift in the peak position for the observed and calculated bands are, respectively, 16 cm^{-1} and ca. 40 cm^{-1}, and is not due to the substitution effect, which is mainly caused by the out-of-plane distortion of the macrocycle resulting from protonation of the N atoms at porphyrin core. Correspondingly, the Raman band associated with the same vibrational motions within FBP, TPP, and TSPP display a similar red shift when compared to diprotonated species (i.e., H_4FBP, H_4TPP, and H_4TSPP). Additionally, the observed shoulders at 1540 cm^{-1} (TPP) and at 1528 cm^{-1} (H_4TSPP) correspond to the calculated peaks at 1555 cm^{-1} and 1529 cm^{-1}, respectively, which results from the ν_a(C_α-C_m-C_α) and θ(C-N(H)-C motions, respectively.

4. Calculated Raman spectra of TPP, H_4TPP, TSPP, H_4TSPP, and H_8TSPP reveal a relatively strong peak around 1238 cm^{-1}, arising from predominantly ν(C_φ-C_m), as well as contribu-

tions from ν_s(C-N(H)-C), ρ(CH) and a comparatively weak $\nu(C_\beta\text{-}C_\beta)$. This vibrational mode is attributed to the measured Raman bands at 1229 cm^{-1} in H_4TSPP spectrum and 1234 cm^{-1} in the TPP. However, in calculated spectra of the unsubstituted free-base porphyrin (FBP and H_4FBP), this peak is respectively red shifted to 1194 and 1217 cm^{-1}, owing to the rocking of the H atom (covalent bounded to *meso*-carbon atom (C_m)), $\rho(C_mH)$, including vibrational bond stretching within the macrocycle (see **Figure 2**). There is a question here we need to answer that while the peak (at 1238 cm^{-1}) is not significantly shifted in the predicted Raman spectra of the diprotonated and/or *meso*-substituted porphyrin molecules, relative to each other, but it is substantially shifted in the FBP and H_4FBP spectra.

This may be explained by the electrostatic repulsive interactions or steric effect between the H atoms covalent bonded to the C_m and C_β atoms in the FBP and H_4FBP structures. The effect decreases with increasing in the distance between the H atoms on the C_β and C_m atoms because of the out-of-plane distortion from planarity in the H_4FBP molecule (diprotonated porphyrin). In the case of *meso*-phenyl or meso-sulfonatophenyl substituted porphyrin molecules, the steric effect between the H atoms on the C_β and C_p (in the *meso*-phenyl substituent) give rise to the rotation of these *meso*-substituted groups about $C_m\text{-}C_\varphi$ bond, in their ground state structure, up to the tilt angle of about 71° and 48° for their unprotonated and protonated structures, respectively. Due to reduced electrostatic repulsion or steric effect by the $C_m\text{-}C_\varphi$ bond rotation, the calculations do not reveal a substantial frequency shift in this peak position (~1238 cm^{-1}) in the *meso*-substituted porphyrin molecules.

(5) In region of 1050–950 cm^{-1}, there are two Raman peaks that are affected by diprotonated and deuterated parent porphyrin molecule. For instance, the observed two peaks at 1002 and 962 cm^{-1} in the TPP spectrum (exc. at 488 nm) are respectively blue shifted to 1016 and 1002 cm^{-1} in the H_4TSPP (exc. at 514 nm). Calculation indicates that the peaks at 1020 and 983 cm^{-1} in the TPP spectrum occurs at 1020 and 986 cm^{-1} in the TSPP. These same bands are blue shifted to 1036 and 1005 cm^{-1} in the calculated spectrum of the protonated-TSPP (H_4TSPP). Our results clearly show that these shifts in the observed peak positions are due to protonation of the porphyrin core that leads to saddle-type distortions of the porphyrin core (i.e., leads to an increase in the degree of freedom of the rocking of the N-H bonds as a consequence of the reduced repulsive interaction or steric effect between these hydrogen atoms). Moreover, GaussView visualization software shows that the peak at 1036 cm^{-1} (in H_4TSPP) is caused by expansion of the pyrrole groups along N(H)…N(H) direction, but in opposite phase (**Figure 2**), as a consequence of $\nu(C_\alpha\text{-}C_\beta)$, which causes the macrocycle to assume a rectangular shape rather than square shape. The band at 1005 cm^{-1} (H_4TSPP) is caused by expansion of the pyrroles along N(H)…N(H) direction likewise macrocycle breathing (or breathing of pyrroles in the same phase) as assigned by Rich and McHale [14].

(6) Another two fundamental Raman bands in the range of low frequency are found at 248 and 338 cm^{-1} in the H_4TSPP spectrum, and at 235 and 365 cm^{-1} in the TPP are respectively attributed to out-of-plane twisting of the macrocycle and breathing of whole molecule, which are in agreement with their experimental values of 242 and 338 cm^{-1} for the H_4TSPP; 235 and 334 cm^{-1} for the TPP. These blue and red shifted bands in the measured and predicted Raman spectrum of the H_4TSPP (dianionic or diprotonated-TSPP) result from the protonation of the

http://dx.doi.org/10.5772/64582

nitrogen atoms at the core, not owing to the *meso*-sulfonato substituted groups. Additional assignments are provided in **Table 1**.

3.1. Isotope effect on the Raman spectrum

The polarized resonance Raman scattering (RRS) spectra, exc. at 488 nm, of the aggregated H_4TSPP (diprotonated TSPP) and deuterated TSPP (D_2TSPP) by Rich and McHale [14] displayed a frequency shifts in the positions of some of the well-known Raman peaks, in addition to changes in the relative intensities of the Raman bands upon deuteration. The authors have reported that the observed Raman bands at 983 and 1013 cm^{-1} in the aggregated H_4TSPP (or diprotonated-TSPP) spectrum are respectively shifted to 957 and 1004 cm^{-1} in the aggregated D_4TSPP spectrum. Additionally, they suggested that these two modes are pyrrole breathing modes and thus these red shifts may be attributed to the substitution of deuterium ions with the labile protons in the porphyrin core [14].

By comparing the spectral positions of these two peaks in the calculated Raman spectra of diprotonated and deuterated porphyrin core with their corresponding nonprotonated ones (see **Table 2**), we see that while the protonated and *meso*-substituted parent porphyrin cause a blue shift in frequency of the two Raman peaks, the deuteration causes a red shift. For example, in the calculated spectrum of the TSPP, while these bands at 1020 and 985 cm^{-1} are blue shifted respectively to 1036 and 1005 cm^{-1} in the H_4TSPP (diprotonated TSPP), they are red shifted to 1012 and 977 cm^{-1} in the D_2TSPP (deuterated TSPP) spectrum, respectively. When all four nitrogen atoms at the porphyrin core are deuterated, these Raman bands are shifted from 1036 and 1005 cm^{-1} (in the H_4TSPP) to 1026 and 983 cm^{-1} in the D_4TSPP (deuterated H_4TSPP), respectively.

For the other moderately intense Raman peaks in the predicted spectrum, the shift in their spectral positions, due to the deuterated nitrogen atoms at the core, is not more than 5 cm^{-1}, which is in agreement with the experimental observation [14]. However, there are several weaker bands in the calculated spectra that displayed a significant shift in frequency (**Figure 1**). The other *meso*-substituted and free-base porphyrin derivatives displayed analogous results, which are in agreement with the experimental findings as argued above. Moreover, the results of calculations suggest that the *meso*-substituted groups do not significantly alter the spectral position of these two Raman bands.

Consequently, the blue shift of the two Raman bands associated with diprotonated nitrogen atoms at the core is not unexpected when considering the steric effect (or electrostatic repulsive effect) between the hydrogen atoms bounded to nitrogen atoms at the core. This effect may be reduced by departing from the planarity of the porphyrin core (or macrocycle) as argued earlier. The red shift also is to be expected because of the isotopic effect since the vibrational frequency is inversely related to the square root of atomic mass that contributes to the vibrational mode. The deuterated nitrogen atoms at the core and one of three oxygen atoms in each of four sulfonato groups (-SO_3D) revealed new Raman peaks in the 2630–2720 cm^{-1} region, which could be an experimental evidence for the presence of the deuterated TSPP (D_4TSPP) or deuterated H_4TSPP (D_8TSPP) in samples.

4. IR spectra of porphyrin and derivatives

We also calculated (at the same level of the DFT) the IR spectra of FBP, TPP, TSPP, H_4FBP, H_4TPP, H_4TSPP, and H_8TSPP, as well as their deuterated structures (D_2FBP, D_2TPP, D_2TSPP, D_4FBP, D_4TPP, D_4TSPP, and D_8TSPP). It is worthy to note that the D_8 represent that the four of eight deuterium atoms covalent bounded to nitrogen at the core and another four bounded to four sulfonato groups (-SO_3D). Calculated spectra exhibit dispersed about the full spectral range many IR features with medium and relatively weak intense, in addition to intense IR bands (see **Figure 3**). The results of the calculations together with their animated motions indicate that the predicted IR vibrational modes are predominantly linked with: (1) symmetric and asymmetric skeletal deformations of the macrocycle and phenyl rings; (2) wagging and rocking of the hydrogen atoms bonded to carbon and nitrogen atoms, CH and NH; and (3) out-of-plane distortion of the phenyl rings and the parent porphyrin or macrocycle. The selected IR bands in the calculated spectra of these compounds studied here are assigned using GaussView animation software. The assigned IR features are given in **Table 3**.

To test the reliability of the calculated IR spectra of the molecules investigated, we compared the IR bands in the calculated spectra of TPP and H_4TSPP (diprotonated TSPP) with experimentally measured IR spectra of TPP [15] and H_4TSPP [16]; as seen in **Table 3**, the spectra correlate quite well. This analysis indicates that the calculated IR spectra of these compounds (FBP/H_4FBP, TPP/H_4TPP, and TSPP/H_8TSPP) are reasonable. We assigned the predicted IR features for the H_4TSPP in connection with the predicted IR spectra of the FBP/H_4FBP, TPP/

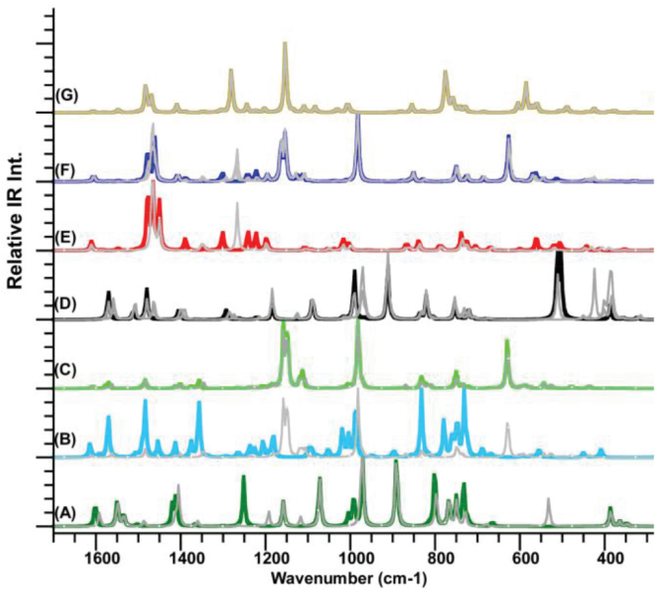


Figure 3. The predicted IR spectra of parent porphyrin and its derivatives: (**A**) free-base porphyrin (FBP) and deuterated FBP (D_2FBP); (**B**) *meso*-tetraphenylporphyrin (TPP) and (D_2TPP); (**C**) anionic *meso*-tetrakis(*p*-sulfonatophenyl)porphyrin (TSPP) and deuterated TSPP (D_2TSPP), and (**D**) diprotonated FBP (H_4FBP) and deuterated H_4FBP (D_4FBP); (**E**) diprotonated TPP (H_4TPP) and deuterated H_4TPP (D_4TPP); (**F**) diprotonated TSPP (H_4TSPP) and deuterated H_4TSPP (D_4TSPP); and (**G**) dicationic TSPP (H_8TSPP) and deuterated H_8TSPP (D_8TSPP). It should be noted that the plotted IR spectra (grey in color) corresponds to that for their deuterated structures. The calculations were carried out in water used as solvent at the B3LYP/6-311G(d, p) level of the theory.

http://dx.doi.org/10.5772/64582

H_4TPP, and TSPP/H_4TSPP/H_8TSPP (in water used as solvent) by taking into account their vibrational motions. Our key conclusions concerning the calculated IR spectra are as following:

1. The predicted IR features at 1603, 1566, 1405, 1193, 1125, 974, and 439 cm^{-1} in the H_4TSPP spectrum are attributable to structural distortion of the *meso*-phenyl substitution, e.g., rocking and/or wagging of hydrogen atoms and bond stretching, no contribution is derived from motions of the sulfonato groups, -SO_3.
2. The following IR bands arise from the vibrational motion of the -SO_3 groups: the most intense IR band at 980 cm^{-1} in the calculated spectrum of the H_4TSPP, which originates from the symmetric stretching of O-S-O bonds, ν_s(O-S-O); one medium intensity at 1151 cm^{-1}, caused by asymmetric stretching of O-S-O, ν_a(O-S-O); and a moderately intense band at 624 cm^{-1} is as a result of bending distortion of the -SO_3 groups, as would describe the closing and opening of an umbrella.
3. A relatively strong IR peak at 1160 cm^{-1} in the spectrum of the H_4TSPP is caused by ν_a(O-S-O) and rocking of CH in phenyl rings, ρ(CH on phenyl).
4. The vibrational motion of the *meso*-sulfonatophenyl rings, ν(S-C), θ(C-C(S)-C) and ρ(CH on phenyl only), produced an IR band with very weak intensity at 1108 cm^{-1}.
5. While the ν(S-C), θ(bending distortion of phenyl), relatively weak wagging of the CH and NH, and twisting of the macrocycle induced an IR peaks at 748 cm^{-1}; twisting of the entire molecule, including bending distortion of the O-S-O bonds and wagging of the CH and NH bonds produced an IR band with very weak intensity at 566 cm^{-1}.
6. The two IR bands with frequencies of ca. 510 and 559 cm^{-1} are indicated as associated with hydrogen atom motions (NH), and are very weak in intensity.
7. A very weak peak at 1089 cm^{-1} is due to the $\rho(C_\beta H)$, which appears essentially at the same spectral position in the calculated IR spectra for the other molecular structures studied here.
8. The calculated IR features, with very weak intensity, at 1386, 1299, 1240, 1036, 848, 825, and 751 cm-1 arise from the bond stretching (ν), rocking (ρ), wagging (w), and bending deformation (θ) of the C and H atoms within macrocycle. These calculated features are found to be spectrally shifted from those in protonated porphyrins, which is in agreement with experimental observation as provided in **Table 3** from references [15] and [16].
9. The peaks at 1004 (weak), 1460 (strong), and 1545 (weak) cm^{-1} are results of symmetric/asymmetric bond stretching, bending deformation, and/or wagging/rocking vibrational motion of the atoms within the porphyrin macrocycle.
10. While in-plane rotational motion of the pyrroline rings, including relatively weak out-of-plane twisting deformation of the phenyl rings, produced weak peak at 439 cm^{-1}; and rocking of phenyl rings and wagging of macrocycle induced a weak IR peak at 427 cm^{-1} in the H_4TSSP spectrum. Another weak one is found at 484 cm^{-1} that originated from the twisting of phenyl and wagging of macrocycle. Complete descriptions for each IR features are provided in **Table 3**.

4.1. Isotopic (or deuteration) effect on the IR spectrum

Calculated IR spectra of the molecules clearly indicate that deuterated porphyrin exhibits relatively intense IR peaks in the range of 2565–2600 cm^{-1}. Such bands are associated with N-D bond stretching. And bands around 2640 cm^{-1} are attributable to O-D bond stretching. The largest frequency shifts are calculated for bands at 540 and 490 cm^{-1} (H_4TSPP, where all N atoms at porphyrin core are protonated) that are shifted to 396 and 366 cm^{-1} in the D_4HTSPP (deuterated-H_4TSPP); in the low-frequency region (below 700 cm^{-1}) bands are attributable to wagging of the N-D bond, w(ND).

In the region of high or mid frequency, where deuterium atom is included in vibrational mode frequency, a red shift in frequency by up to 10 cm^{-1} is shown in the D_2TSPP. Deuteration also has an influence on the intensity of the IR bands; see **Figure 3**. Shift in the region of high frequency of D_2FBP, D_4FBP, and D_4TPP spectra are more significant than those in the spectra of the D_2TSPP and D_4TSPP. These results imply that above the low-frequency region, the frequency shifts as a result of the deuteration decrease with increasing size of the substituent group.

5. Solvent effect on the IR spectrum

We investigated the solvent effect on the IR spectrum of the H_4TSPP by using toluene, dimethyl sulfoxide (DMSO) and water as a solvent. Calculations indicate that below 1100 cm^{-1} there is no significant frequency, shift in peak positions H_4TSPP, but above 1100 cm^{-1} shifts do occur. Specifically, the IR peak centered at around 1200 cm^{-1} is shifted to 1188 cm^{-1} (toluene), 1166 cm^{-1} (DMSO), and 1160 cm^{-1} (water). Also, the IR peaks centered about 1453 and 1477 cm^{-1} in the gas phase spectrum are shifted to 1468 and 1490 cm^{-1} (toluene), 1480 and 1497 cm^{-1} (DMSO), and 1481 and 1499 cm^{-1} (water), respectively. This observation suggests that the IR features, especially in high energy region, of the parent porphyrin and its derivatives, at least for H_4TSPP, are responsive to its surroundings.

6. Resonance Raman spectra of aggregated diprotonated-TSPP

In the section, we will discuss the results vibroelectronic properties of the aggregated-H_4TSPP (known as acidic-, dianionic-, or diprotonated-TSPP). Several structural and spectroscopic studies have shown that TSPP aggregates in acidic aqueous solution. **Figure 4** shows the absorption spectra of free-base TSPP (pH = 12), H_4TSPP (pH = 4.5), and aggregated H_4TSPP (pH = 1.6), with concentration of 5×10^{-5} M in aqueous solution.

While the spectrum of the TSPP [17] exhibited a Soret band at 410 nm and several weak Q bands in the region of 500–640 nm, the monomeric H_4TSPP spectrum exhibited the Soret band at 432 nm, and Q-bands at 594 and 642 nm. **Figure 4** shows the Soret band of the H_4TSPP is split into H- and J-band components in the H_4TSPP aggregate as a sharp and intense absorption

http://dx.doi.org/10.5772/64582

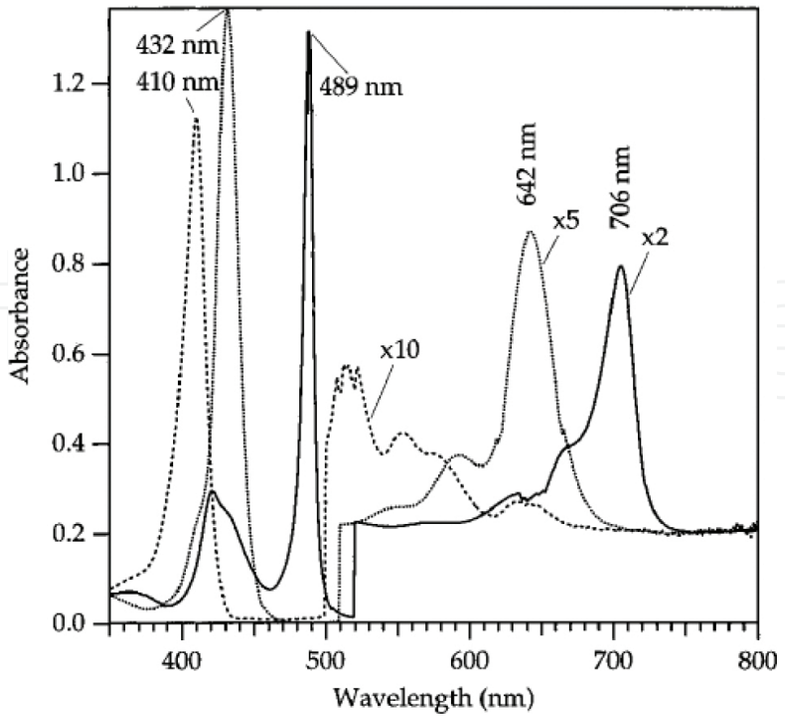


Figure 4. UV-vis spectra of the free-base TSPP (the maximum of the absorption band at 410 nm), monomeric H_4TSPP (the maximum at 432 nm) and aggregated H_4TSPP (the maximum at 489 nm) [20]. The concentration of compounds in each case is 5 × □ 10^{-5} M in the aqueous solution. The pH = 12 for the free-base TSPP; pH = 4.5 for the monomeric H_4TSPP; pH = 1.6 for the aggregated H_4TSPP, and [KCl] = 0.1 M. Spectra above ca. 500 nm have been offset by +0.2 absorbance units and amplified by the indicated factor to aid presentation. The structure on the band at around 500 nm for the free-base TSPP is an artifact attributable to the absorption spectrometer.

band at 489 nm (J-aggregate) and a broad and weak absorption band at 422 nm (H-aggregate) are formed. The Q-bands at 594 and 642 nm (in the monomeric H_4TSPP) is also shifted to ca. 670 and 706 nm in the aggregated H_4TSPP spectrum, respectively. The UV-vis spectra results suggest that aggregation evolves through the formation of diprotonated TSPP (H_4TSPP), and only occurs at a pH below 5. These observations have also reported by other researchers [18, 19].

Figure 5 presents the Raman spectra of free-base (TSPP), monomeric dianion (H_4TSPP) and aggregated H_4TSPP resonantly excited at their respective Soret-band absorption wavelengths (**Figure 4**). Analysis of the resonance Raman (RR) spectra of the H_4TSPP and aggregated H_4TSPP reveal the presence of bands that do not accommodate bands of the free-base porphyrin. However, an in-depth examination indicates that subtle differences bands of the aggregate and the dianionic monomer are correlated. The most important correlation in spectra is found in the low-frequency region, where two bands of dianionic TSPP monomer at 233 and 310 cm^{-1} correlate with two dramatically enhanced aggregate bands at 241 and 317 cm^{-1}, in addition to two weak satellite bands at 205 and 362 cm^{-1}.

Moreover, DFT calculations (at B3LYP/6-311G(d, p) level) show that while the band at 317 cm^{-1} is due to breathing of the whole molecule, the enhanced band at 241 cm^{-1} results from the out-of-plane wagging of the macrocycle. Hence, computationally these two Raman bands of porphyrins originate from out-of-plane modes—in conjunction with bending of the C_m-ph

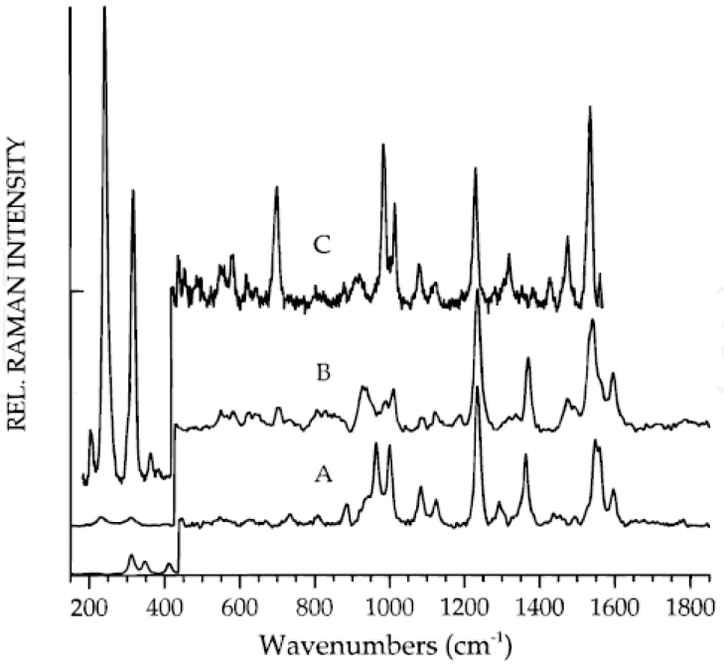


Figure 5. Resonance Raman spectrum (RRS) of the TSPP [20]: (A) free-base TSPP, exc. at = 416 nm; (B) diprotonated TSPP (H_4TSPP), exc. at 432 nm; (C) aggregated H_4TSPP, exc. at 488 nm. Where the solutions used here were the same as used for the measured absorption spectra in **Figure 4**.

bond (ph representing phenyl) and deformation of the core of the porphinato macrocycle caused by pyrrole ring tilt and swivel [20–22]. Moreover, in the case of lanthanide sandwich dimer porphyrins, low-frequency Raman bands have been hypothesized to reflex the degree of intramolecular π-π interaction and to be connected with the intradimer vibration that modulates the separation between the two porphyrin moieties, or owing to symmetrical linear combinations of out-of-plane distortions of the neighboring porphinato macrocycles [23].

Given the enhancement of scattering associated with bands having motions that can strongly couple with excitonic motion, which helps define the aggregate's structure, we report in **Table 1** assignments made through such a scheme and by comparison to the literature. It is to be noted that a theoretical construct known as "aggregation-enhanced Raman scattering (AERS)," has been advanced by one of us (DLA) to explain which bands would experience significant enhancement upon aggregation of the scattering species. And, indeed, the two bands discussed above that show enormous enhancement upon aggregation of H_4TSPP have motions that couple to exciton movement through the aggregate and would be expected to experience significantly enhanced Raman intensities [12].

Acknowledgements

We would like to thank Ömer Andaç (Chemistry Department of Ondokuz Mayıs University) for kindly providing computing facilities and software expertise. We also thank staff at TUBITAK ULAKBIM, the high performance and Grid Computing Center (TR-Grid e-Infra-

structure), for performing the calculations reported herein. Also, we would like to thank the U.S. National Science Foundation (NSF) for support of research efforts under grant No. HRD-08-33180.

Author details

Metin Aydin[1*] and Daniel L. Akins[2]

*Address all correspondence to: aydn123@netscape.net

1 Department of Chemistry, Faculty of Art and Sciences, Ondokuz Mayıs University, Samsun, Turkey

2 Department of Chemistry and Biochemistry, Center for Analysis of Structures and Interfaces (CASI), The City College of the City University of New York, New York, USA

References

[1] Shelnutt, J. A. Thesis: Resonance Raman spectroscopy of manganese (III) Etioporpyrin I: Theory and experiment, Georgia Institute of Technology, November, 1975.

[2] Albrecht, A. C. On the theory of Raman intensities, J. Chem. Phys., 1961, 34, 1476–1484.

[3] Warshel, A.; Dauber, P. Calculations of resonance Raman spectra of conjugated molecules, J. Chem. Phys., 1977, 66, 5477–5488.

[4] Polavarapu, P. L. Ab initio vibrational Raman and Raman optical activity spectra, J. Phys. Chem., 1990, 94, 8106–8112.

[5] O'Boyle, N. M.; Tenderholt, A. L.; Langner, K. M. cclib: A library for package-independent computational chemistry algorithms, J. Comp. Chem., 2008, 29, 839–845.

[6] Kasha, M. Energy transfer mechanisms and the molecular exciton model for molecular aggregates, Radiat. Res. 1963, 20, 55.

[7] Okamura, M. Y.; Feher, G.; Nelson, N. Chapter 5: Reaction centers in *Photosynthesis*, Govindjee, Ed. Academic Press: New York, 1982, pp. 195–272.

[8] Pearlstein, R. M. Amesz, J. (Ed.) Chapter 13: Structure and exciton effects in photosynthesis. Elsevier: Amsterdam, 1987, pp. 299–317.

[9] O'Neil, M. P.; Niemcyzk, M. P.; Svec, W. A.; Gosztola, D.; Gaines III, G. L.; Wasielewski,M. R. Picosecond optical switching based on biphotonic excitation of an electron donor-acceptor-donor molecule, Science, 1992, 257, 63.

[10] Wagner, R. W.; Lindsey, J. S.; Seth, J.; Palaniappan, V.; Bocian, D. F. Molecular optoelectronic Gates, J. Am. Chem. Soc., 1996, 118, 3996.

[11] Aydin, M. Comparative study of the structural and vibroelectronic properties of porphyrin and its derivatives. Molecules, 2014, 19, 20988–21021.

[12] Akins, Daniel L., Enhanced Raman scattering by molecular nanoaggregates (Invited Review Article), nanomater. Nanotechnol, 2014, 4, 4. DOI: 10.5772/58403

[13] Aydin, M. DFT and Raman spectroscopy of porphyrin derivatives: Tetraphenylporphine (TPP). Vib. Spectrosc. 2013, 68, 141–152.

[14] Rich, C. C.; McHale, J. L. Influence of hydrogen bonding on excitonic coupling and hierarchal structure of a light-harvesting porphyrin aggregate. Phys. Chem. Chem. Phys. 2012, 14, 2362–2374.

[15] Mi, Z.; Guo-Hui, L.; Shu-Qin, G.; Zuo-wei, Li. Infrared spectroscopic investigations of J-aggregates of protonated tetraphenylporphine. Chem. Res. Chin. Univ., 2009, 25, 257–260.

[16] Zhang, Y.H.; Chen, D.M.; He, T.; Liu, F.C. Raman and infrared spectral study of meso-sulfonatophenyl substituted porphyrins (TPPSn, n_/1, 2A, 2O, 3, 4). Spectrochim. Acta Part A, 2003, 59, 87–101.

[17] Akins, D. L.; Zhu, H.R.; Guo, C., Absorption and Raman scattering by aggregated meso-tetrakis(p-sulfonatophenyl) porphine. J. Chem. Phys., 1994, 98, 3612–3618.

[18] Pasternack, R. F.; Huber, P. R.; Boyd, Engasser, P.; Francesconi, G.; Gibbs, L.; Fasella, E.; Venturo, P.; Cerio, G.; Hinds, L. deC. On the aggregation of meso-substituted water-soluble porphyrins, J., Am. Chem. Soc., 1972, 94, 4451.

[19] Ohno, O.; Kaizu, Y.; Kobayashi, H. *J*-aggregate formation of a water-soluble porphyrin in acidic aqueous media, J. Chem. Phys., 1993, 99, 4128.

[20] Akins, D. L.; Özçelik, S.; Zhu, H. R.; Guo, C. Fluorescence decay kinetics and structure of aggregated tetrakis(*p*-Sulfonatophenyl)porphyrin, J. Chem. Phys. 1996, 100, 14390–14396.

[21] Choi, S.; Spiro, T. G. Out-of-plane deformation modes in the resonance raman spectra of metalloporphyrins and heme proteins, J. Am. Chem. Soc. 1983, 105, 3683.

[22] Alden, R. G.; Crawford, B. A.; Doolen, R.; Ondrias, M. R.; Shelnutt. J. A. Ruffling of nickel(II) octaethylporphyrin in solution, J. Am. Chem. Soc. 1989, 111, 2070.

[23] Donohoe, R. J.; Duchowski, J. K.; Bocian, D. F. Hole delocalization in oxidized cerium(IV) porphyrin sandwich complexes, J. Am. Chem. Soc. 1988, 110, 6119.